Journal of Catalysis 436 (2024) 115597

Contents lists available at ScienceDirect

Journal of Catalysis

journal homepage: www.elsevier.com/locate/jcat

Research article

Covalent stabilization of copper porphyrin into carbon nitride for the catalytic reduction of CO_2

Claudio Cometto [a], Giulia Marafon [a,1], Verónica Celorrio [b], Gonzalo García [c], Steffi Y. Woo [d], Enrico Paron [a], Alberto Zobelli [d], Gregorio Bottaro [e], Lidia Armelao [a,f], Elena Pastor [c], Alessandro Moretto [a], Laura Calvillo [a,*]

[a] Dipartimento di Scienze Chimiche, Università di Padova and INSTM Research Unit, Via Marzolo 1, 35131 Padova, Italia
[b] Diamond Light Source Ltd, Diamond House, Harwell Science and Innovation Campus, Didcot, Oxfordshire OX11 0DE, United Kingdom
[c] Instituto Universitario de Materiales y Nanotecnología, Universidad de La Laguna, Astrofísico F. Sánchez s/n, La Laguna, Tenerife 38071, Spain
[d] Université Paris-Saclay, CNRS, Laboratoire de Physique des Solides, 91405 Orsay, France
[e] CNR-ICMATE and INSTM, Dipartimento di Scienze Chimiche, Università di Padova, via Marzolo 1, I-35131, Italy
[f] Department of Chemical Sciences and Materials Technology (DSCTM), Consiglio Nazionale delle Ricerche Piazzale A. Moro 7, 00185 Roma, Italy

ARTICLE INFO

Keywords:
Co-polymerization synthesis
CO_2 reduction
Heterogeneous molecular catalyst
DEMS
in situ XAS

ABSTRACT

The development of active, selective, and durable (photo)electrocatalytic hybrid systems by combining molecular catalysts and semiconductor substrates is crucial for efficiently converting solar light into high-value products. Herein, a one-step synthesis method to obtain carbon nitride (CN) nanosheets, which allows the direct covalent polymerization with molecular catalysts, was developed. Copper-porphyrin (CuPor) units were embedded in the CN structure as a case-study. The single and hybrid materials were fully characterized by combining microscopic and spectroscopic techniques and tested as (photo)electrocatalysts for the CO_2 reduction reaction (CO_2RR) in aqueous solution. Experimental evidence confirmed an effective boost of the CN photoelectrocatalytic activity by introducing the CuPor units. Formate was identified as the only CO_2RR product on both CuPor and CuPor-CN, simultaneously with hydrogen from the competitive hydrogen evolution reaction. However, the formate/hydrogen ratio was higher when the hybrid material was used as catalyst, suggesting a synergetic effect between CuPor and CN, that favors the CO_2RR and hinders the HER. In addition, the stability of the CuPor units in the CN matrix under catalytic conditions was studied by *in situ* X-ray absorption. No changes of the Cu porphyrin structure or formation of copper clusters/nanoparticles was observed as a function of the applied potential nor after an accelerated ageing treatment, suggesting that the CN matrix is able to stabilize the Cu sites avoiding their agglomeration.

1. Introduction

The use of hybrid systems that combine molecular catalysts and semiconductor supports has emerged as a promising approach to obtain active, selective, and durable catalysts capable of efficiently converting clean energy into high-value products (e.g. hydrogen production or CO_2 recycling) [1–3]. In this context, the use of carbon nitride (CN) as substrate for the immobilization of molecular catalysts entails an interesting strategy since it allows for the use of solar light to perform and/or enhance the catalytic processes [4,5].

CN is an organic polymer mainly constituted by carbon and nitrogen atoms with a structure very similar to that of graphene. It consists of stacked two-dimensional (2D) sheets, but it contains a high amount of graphitic nitrogen that opens its electronic band gap (2.7 eV), making CN a photoactive material able to absorb visible light more efficiently than the commonly used TiO_2 [6,7]. For this reason, CN constitutes a new class of multifunctional platform for electronic, catalytic and energy applications [8,9].

Several strategies have been reported in the literature for the synthesis of CN: (i) chemical vapor deposition [10,11]; (ii) pyrolysis of nitrogen-rich precursors [12]; (iii) shock-compression synthesis [13,14]; and (iv) ionothermal condensation [15,16]. All these methods require

* Corresponding author.
E-mail address: laura.calvillolamana@unipd.it (L. Calvillo).
[1] Present address: Carbogen Amcis, Hauptstrasse 171, 4416 Bubendorf, Switzerland.

https://doi.org/10.1016/j.jcat.2024.115597
Received 1 March 2024; Received in revised form 17 May 2024; Accepted 5 June 2024
Available online 6 June 2024
0021-9517/© 2024 The Author(s). Published by Elsevier Inc. This is an open access article under the CC BY-NC-ND license (http://creativecommons.org/licenses/by-nc-nd/4.0/).

high temperatures (500 – 600 °C) and yield a bulk material, which requires a subsequent exfoliation step in order to obtain the two-dimensional (2D) material. In this work, we have developed a new synthesis method that requires low temperature (150 °C) and directly yields CN nanosheets.

As said above, CN constitutes an excellent substrate for immobilizing molecular catalysts. Usually, the catalytic units are coupled with CN through electrostatic interactions or π-π stacking [1–3,5]. However, the coupling by covalent bonding encourages an improved electron transfer between the substrate and the catalytic unit, increasing the efficiency of the energy utilization. Some works in this direction can be found in the literature, even if the functionalization process is a difficult task [17–21]. Both the molecule and the support must be precisely designed to allow their interaction, and an appropriate coupling route must be finely planned to maintain the intrinsic properties of both units.

The low-temperature synthesis method developed in this work, on the contrary, allows the direct co-polymerization of molecular catalysts and CN precursors, avoiding the second functionalization step. The consequence is the introduction of the catalytic unit into the CN structure, resulting in a very close contact between the photoactive platform (CN) and the catalytic centers (molecular catalyst), as well as a good dispersion of the catalytic units into the semiconductor matrix. The one-step process makes this approach suitable and very versatile for the synthesis of hybrid materials.

In this work, for the first time, we have used a one-pot synthesis procedure to prepare an heterogenous molecular catalysts. With this aim, we have added copper-*meso*-tetrakis-(p-NH_2phenyl)porphyrin (CuPor) to the CN precursors mixture to obtain a hybrid material with the metal-porphyrin embedded in the CN matrix (CuPor-CN). Metal phthalocyanines and porphyrins are among the most popular molecular catalysts for the photocatalytic reduction of CO_2 [22–25]. They present the possibility to fine-tune the catalytic activity by varying the type of metal ions and organic ligands, which gives them diverse electron-donating and transporting properties [26–28]. Their photocatalytic activity has been extensively studied in the literature, while the electrocatalytic one has been less explored. In addition, little attention has been paid to the study of the durability of such electrocatalysts, which is their main issue. This type of molecular catalysts or their hybrid materials are usually characterized by a poor long-term stability under electrocatalytic conditions, since the metal atoms tend to migrate and form clusters/nanoparticles [25,29–32]. In this work, we have tested the hybrid materials as (photo)electrocatalysts for the CO_2 reduction reaction (CO_2RR), benefiting from the close contact and the consequent improved electron transfer between the photoactive platform (CN) and the catalytic centers (copper atoms in porphyrins) through the covalent bonds. The analysis of the products was carried out by rotating ring disk electrode (RRDE) measurements and differential electrochemical mass spectrometry (DEMS). The hybrid material was able to reduce CO_2 to formate from −0.4 V vs RHE, while CN produced only H_2 in the same conditions. Commercial CuPor produced the same products than the hybrid material but with a higher hydrogen:formate ratio. In addition, we have investigated the stability of the copper-porphyrin units embedded into the CN matrix under catalytic conditions by *in situ* XAS measurements. No changes of the Cu porphyrin structure or formation of copper clusters/nanoparticles were observed as a function of the applied potential and after an accelerated ageing treatment, suggesting that the CN matrix is able to stabilize the Cu sites avoiding their agglomeration.

2. Experimental

2.1. Synthesis of 2D carbon nitride (CN)

1.26 g (0.01 mol) of melamine, 1.84 g (0.01 mol) of cyanuric chloride, and 12.24 g (0.18 mol) of imidazole were mixed in solid form in a round flask. The temperature was increased up to 150 °C under stirring using a heating ramp of 4 °C min^{-1}. At this temperature, imidazole liquefied providing a polymerization concentration of 0.8 M for each monomer. Rapidly, the solution became highly viscous, and the polymerization was allowed to proceed for 3 h. Then, the mixture was cooled down naturally to room temperature and 100 ml of deionized water was added under stirring. The precipitate was collected by filtration (gooch filter porosity 4) and washed several times with water, dimethylformamide (DMF), ethanol and acetonitrile. The so obtained product (1.7 g) was dried under vacuum in a desiccator.

2.2. Synthesis of copper-porphyrin modified carbon nitride (CuPor-CN) hybrid materials

Typically, 0.42 g (3 mmol) of melamine, 0.61 g (3 mmol) of cyanuric chloride, 0.05 g (0.074 mol) of (Cu^{2+})H_2T(4-NH_2PP), and 4.1 g (0.06 mol) of imidazole were mixed in solid form in a round flask equipped with a magnetic stirrer. The temperature was increased up to 150 °C under stirring using a heating rate of 4 °C min^{-1}. The polymerization was left to proceed for 3 h. The mixture was allowed to cool down to room temperature and 50 ml of distilled water was added under stirring. The precipitated was collected by filtration (gooch filter porosity 4) and washed several times with water, DMF, chloroform and acetonitrile. The so obtained product (0.5 g) was dried under vacuum in a desiccator. The product was labelled as CuPor-CN. The amount of copper in the hybrid material was determined by TGA experiments in Ar atmosphere, being 0.6 wt% Cu (3.8 wt% Cu-porphyrin). The synthesis of the amino-modified porphyrin, (Cu^{2+})H_2T(4-NH_2PP), is described in the Electronic Supporting Information (ESI).

2.3. Characterization techniques

Transmission electron microscopy (TEM) images were acquired with a FEI Tecnai G12 microscope, while scanning TEM (STEM)-electron energy-loss spectroscopy (EELS) was performed on a Nion UltraSTEM 200 microscope operated at 60 keV using the relative quantification methods (N_C/N_N atomic ratio) [33]. The scattering cross-sections of the C *K* and N *K*-edges collected simultaneously were calculated using the Hartree-Slater models available within DigitalMicrograph based on the scattering geometry parameters used (33 mrad convergence semi-angle and 40 mrad collection semi-angle). Samples were prepared by dispersing the powder in methanol and successive drop-casting onto a TEM grid.

X-ray photoelectron spectroscopy (XPS) was performed in a custom-made UHV system working at a base pressure of 10^{-10} mbar, equipped with an Omicron EA125 electron analyzer and an Omicron DAR 400 X-ray source with a dual Al − Mg anode. Core-level photoemission spectra (C 1 s, N 1 s, O 1 s, and Cu 2p) were collected at room temperature with a non-monochromatized Al K_α X-ray source (1486.3 eV). Single spectra were acquired using 0.1 eV steps, 0.5 s collection time, and 20 eV pass energy. In order to analyze the single components of the C 1 s and N 1 s regions, the spectra were separated into chemically shifted components. For the C 1 s region, an asymmetrical shape was used for the sp^2 component, whereas symmetrical Voigt functions were used for the sp^3 component, the C-O functional groups and C-$(N)_3$ species. For the N 1 s region, symmetrical Voigt functions were used.

X-ray adsorption measurements were recorded on beamline B18 at Diamond Light Source (UK) with ring energy of 3 GeV and a current of 300 mA. The monochromator used was Si(1 1 1) crystals operating in Quick EXAFS (QEXAFS) mode. Pellets of commercial copper porphyrin (CuPor, Sigma-Aldrich) and CuPor-CN were measured in transmission mode at the Cu K (8979 eV) absorption edge at 298 K. The Cu foil was measured simultaneously. Calibration of the monochromator was carried out using the Cu foil before the measurements. The acquired data were processed and analyzed using the Athena and Artemis programs, respectively, which implement the FEFF6 and IFEFFIT codes. For the *in situ* XAS measurements, the samples were prepared as button electrodes (fresh electrodes). The samples were placed in an electrochemical cell

(available at B18) as working electrode, using a Pt wire and a calomel electrode as counter and reference electrode, respectively. The measurements were performed at four different applied potentials both in N_2– and CO_2-saturated 0.1 M $KHCO_3$, pumped through the cell using a peristaltic pump. The cell was connected to a potentiostat to control the applied potential during the XAS measurements. In addition, samples subjected to an accelerated ageing treatment (AAT, 1000 cycles between + 0.2 and −0.9 V_{RHE} at 50 mV s^{-1}) were *ex situ* measured.

Solid state absorption spectra were recorded using a Cary 5000 UV–Vis-Spectrometer equipped with a Diffuse Reflectance Accessory consisting in an integrating sphere. The spectra were acquired and plotted as Kubelka-Munk function F(R) = A*C/S (A = absorbance, C = Concentration, S = scattering coefficients). The spectra were normalized at wavelengths corresponding to the maximum of Soret band for CuPor (solid state) and CuPor-CN, or the maximum of the CN spectrum. The spectrum of CuPor in DMF solution was acquired with the same instrument using the transmission acquisition geometry. The spectrum was then normalized at the maximum of Soret band.

Electrochemical measurements were conducted in a three-electrode cell using a saturated calomel electrode (SCE) as reference electrode and a graphite rod as counter electrode. The potentials in this work have been converted to a reversible hydrogen electrode (RHE). The working electrode consisted in a thin-film catalyst layer (66 μg cm^{-2}) deposited on a glassy carbon (GC) electrode (3 mm diameter). The catalyst ink drop-cast on the GC was prepared by mixing 2 mg of catalyst, 40 μL Nafion® (5 wt%, Sigma-Aldrich), 500 μL dimethylformamide (DMF) and 500 μL Milli-Q water. The ink was sonicated for 20 min to facilitate the dispersion of the catalyst. Measurements were carried out in Ar- and CO_2-saturated 0.1 M $KHCO_3$, prepared from high purity reagents (Sigma-Aldrich). The samples were characterized by cyclic voltammetry (CV) and linear sweep voltammetry (LSV) to determine the activity towards the CO_2RR. The measurements were recorded in absence and presence of light, using a white LED lamp (OSRAM – 9 LED Star Oslon 150 white 1170 lm/cm^2@350 mA) as light source, to investigate the activity enhancement by light. All the experiments were performed at room temperature. The currents reported are normalized by the electrode geometric area.

A rotating ring-disk electrode (RRDE) with a glassy carbon disk (5 mm diameter) and platinum ring was used for the characterization of the products obtained during the CO_2RR [34,35]. Two types of measurements were performed: (i) the ring was cycled between + 0.2 V and + 1.6 V vs RHE at 0.2 Vs^{-1}, while the disk was held at different potential values between −0.6 V and −1.15 V vs RHE; and (ii) the ring was held at + 0.8 V vs RHE, while the disk was cycled between −0.1 V and −1.05 V vs RHE. Measurements were performed at 3500 rpm.

A scheme of the DEMS setup used for the *in situ* spectrometric and electrochemical measurements is described in detail in ref. [36]. Briefly, the working electrode (WE) was fixed between a PTFE membrane (Scimat) and a glassy carbon rod, which also keeps the electrical contact. The cell was designed to follow "in-situ" the electrochemical properties of electrodes and, simultaneously, the gaseous species produced on the electroactive surface through mass spectrometry. Thus, the experimental setup allows the simultaneous acquisition of mass spectrometric cyclic voltammograms (MSCVs) for selected *m/z* (mass to charge) ratios and conventional cyclic voltammograms (CVs), as well as mass spectrometric transients (MST) for selected *m/z* ratios and conventional current transients (CTs). Electrochemical experiments were carried out in a three-electrode electrochemical cell at room temperature and atmospheric pressure. The counter electrode was a high surface area carbon rod and the reference electrode was a reversible hydrogen electrode (RHE) placed inside a Luggin capillary. The potentiostat–galvanostat used was an Autolab PGSTAT302 (Ecochemie). The spectroelectrochemical cell was directly attached to the vacuum chamber of a mass spectrometer (Balzers QMG112) with a Faraday cup detector. The working electrode was immersed into 0.1 M $KHCO_3$ electrolyte solution, which was deaerated with argon (N50). In order to analyze the activity of catalysts towards the reduction of CO_2, previously to each measurement, CO_2 (99,99 %, Air Liquide) was bubbled during 30 min. In both atmospheres (Ar and CO_2), a CV and MSCV were initially recorded following the ionic currents associated with a large variety of possible CO_2RR products, as well as CN decomposition products, in order to elucidate the species generated. The signals recorded in Ar-saturated electrolyte were $m/z = 2$, $m/z = 14$, $m/z = 16$, $m/z = 28$, $m/z = 44$, and $m/z = 45$, related to the formation of hydrogen, CO, CH_4, CO_2, or any product that could be confused with the expected formate. During this initial screening, only the signal related to the formation of hydrogen ($m/z = 2$) from the HER was observed. This result allowed us to exclude the decomposition of the CN substrate or the Cu porphyrin units in the potential window studied. Subsequently, additional CVs and CTs, with the corresponding MSCV and MST, were recorded only following the $m/z = 2$. In CO_2-saturated electrolyte, the signals recorded during the first CV and MSCV were $m/z = 2$ (H_2), $m/z = 16$ (CH_4), $m/z = 28$ (CO), $m/z = 29$, $m/z = 30$ (C_2H_6), $m/z = 31$ (CH_3O^-), and $m/z = 45$ ($HCOO^-$). The only signals detected were those corresponding to the formation of hydrogen and formate. Therefore, they were the only signals registered in the subsequent MSCVs and MSTs measurements.

3. Results and discussion

A new synthesis method for the direct preparation of CN nanosheets at low temperature has been developed. Cyanuric chloride, melamine and imidazole powders were mixed and heated up to 150 °C. At this temperature, imidazole is a liquid and acts as solvent and base but also as template. Therefore, cyanuric chloride and melamine polymerize in between the imidazole layers, resulting directly in nanosheets. To prove the success of the new synthesis method, the results of the new CN have been compared to those of the material obtained by the conventional thermal synthesis (T-GCN). The complete characterization of the CN substrate, as well as the synthesis and characterization of the conventional T-GCN, can be found in the ESI (Figures S1-S7 and Tables S1 and S2).

Cu-amino-porphyrin was introduced into the CN structure through the co-polymerization of the porphyrin units and the CN precursors. The success of the copper-porphyrin incorporation into the CN matrix was proved by X-ray absorption spectroscopy (XAS). The X-ray absorption near-edge structure (XANES) data and the corresponding Fourier-transform extended X-ray absorption fine structure (FT EXAFS) spectra for CuPor-CN are reported in Fig. 1a and 1b, respectively. The analysis of the XANES region indicates that the oxidation state of Cu is + 2 for both CuPor-CN and the commercial copper porphyrin (CuPor, Sigma-Aldrich). CuPor displays a pre-edge peak at 8985 eV, associated to the 1 s → $4p_z$ transition of the square-planar Cu-N_4 structure [25,37]. The XANES spectra of CuPor-CN is very similar to that of CuPor, indicating that the metal porphyrin units maintain the original structure in the hybrid material. The corresponding FT EXAFS for both materials show an intense peak at 1.5 Å, attributed to the first coordination Cu-N_4 shell, while additional peaks at R > 2.5 Å are due to carbon atoms in the porphyrin ring. No peaks attributed to Cu-Cu interactions are observed at 2.2 Å; therefore, the decomposition and/or agglomeration of CuPor units can be excluded. The stability of the porphyrin structure inside the CN matrix was further confirmed by fitting the EXAFS data (Table S3). In both samples, Cu has four nitrogen neighbor atoms at 1.97 Å, in agreement with the data reported in the literature [37].

The oxidation state of copper in the hybrid material was confirmed by XPS. CuPor-CN shows two peaks in the Cu 2p region at 933.4 eV and 953.1 eV (Fig. 1c), corresponding to the Cu $2p_{3/2}$ and Cu $2p_{1/2}$ spin–orbit states, characteristic of Cu(II) in the porphyrin ring [38]. For the commercial CuPor, additional peaks at 935.6 eV and 954.9 eV are observed, which could be attributed to the presence of Cu(III)Por at the surface [38]. The C 1 s and N 1 s regions of the commercial CuPor, pristine CN, and CuPor-CN were also analyzed and the results are reported in Fig. 1d-1e and Tables S1, S2, S4 and S5. The C 1 s spectrum of

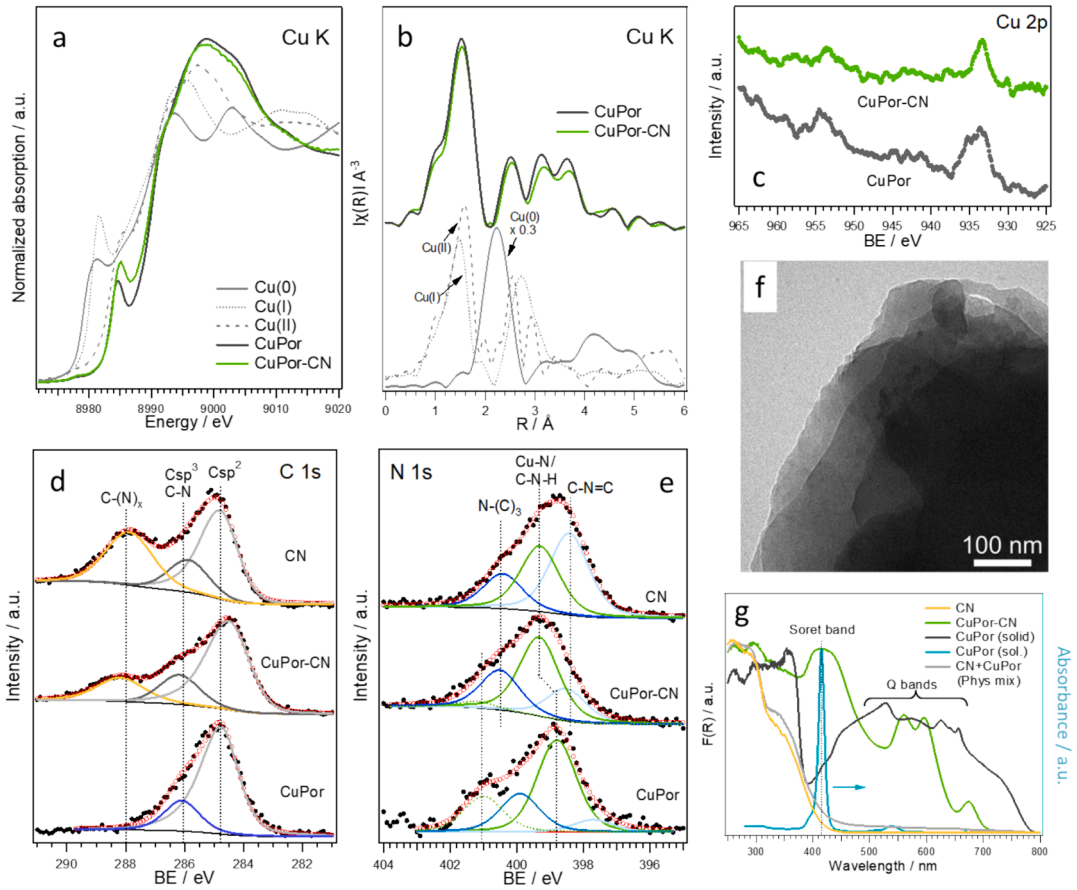

Fig. 1. Physicochemical and optical characterization of CN and CuPor-CN: (a) XANES and (b) corresponding FT EXAFS spectra at the Cu K edge for CuPor-CN and commercial Cu porphyrin; (c) Cu 2p, (d) C 1 s, and (e) N 1 s XPS regions; (f) representative TEM image of CuPor-CN; and (g) UV–Vis diffuse reflectance spectra for CN, CuPor-CN and the commercial CuPor. The references used for the determination of the Cu oxidation state are also shown in (a) and (b). The deconvolution of the C 1 s and N 1 s XPS regions into chemically shifted components has been included in (d) and (e).

CN shows the characteristic component of the CN materials at 287.8 eV, attributed to C-$(N)_3$, which should be the main component for this kind of material [39,40]. However, two additional components are observed in the C 1 s region at 284.8 eV and 286.0 eV related to the C sp^2 and C sp^3/C-N components. A small amount of C sp^2 was also observed by EELS (Figure S6), and could be related to the presence of imidazole in the final product, since the synthesis temperature is not high enough to suggest the loss of nitrogen atoms and formation of C = C bonds. Since no C sp^3 was detected by EELS, this component can be related to the presence of adventitious carbon from the sample holder, which is visible due to the very thin film of sample deposited to avoid charging effects. CuPor-CN also shows the characteristic component of carbon nitride at 288.0 eV. An increase of the C sp^2 and C-N (overlapping with C sp^3) components, compared to the C-$(N)_3$ component, is observed. This increase can be attributed to the presence of the porphyrin units. The N 1 s region of the pristine CN can be deconvolved into three main components at 398.4 eV, 399.3 eV and 400.4 eV, related to C-N = C, C-N–H and N-$(C)_3$ nitrogen species, respectively [40]. CuPor-CN shows the same nitrogen components as CN but, in this case, the component at 399.3 eV overlaps with the Cu–N component of the CuPor units at 399.0 eV, as observed in the N 1 s spectrum of the commercial porphyrin [41]. The N 1 s spectrum of CuPor contains three peaks at 397.9 eV, 400.1 eV and 401.3 eV related to = N-, –NH-, and the expected Teller effect for copper porphyrins [38,41].

Fig. 1f shows a representative TEM image of CuPor-CN. By comparing Fig. 1f and S4b, it can be said that the addition of CuPor does not alter the morphology of CN, which presents 2D flakes ranging from few hundreds of nanometers up to a few micrometers (Figures S6 and S7). The thickness can be as thin as few tens of nanometers, as it can be roughly estimated from contrast in STEM HAADF images (Figures S6c, d). The same morphology is preserved in the CuPor-CN, as observed by TEM images (Fig. 1f and S7). Additional TEM images confirming the polymeric nature of the samples can be found in Figure S7.

Finally, the light absorption of the pristine and CuPor-modified CN was investigated by UV–Vis diffuse reflectance absorption spectroscopy (Fig. 1g). CN shows an absorption edge at around 420 nm, attributed to the π-π^* electron transitions in the conjugated aromatic system, in agreement with the data reported in the literature [42]. The incorporation of the CuPor into the CN structure results in a significant enhancement of the visible light absorption in the 400–690 nm range. To analyze the new bands upon the incorporation of CuPor, the absorption spectra of the CuPor in solid state and in solution (in dimethylformamide) are included in Fig. 1g. In both solid and solution spectra, the characteristic Soret and Q bands of porphyrins are observed [42,43]. In solid state, a blue shift and a broadening of the Soret band, in comparison with the spectrum in solution, are observed. The blue shift is typical of porphyrin aggregates with a cofacial arrangement [5,44–47]. Noteworthy, the bands corresponding to the presence of porphyrin in the CuPor-CN spectrum resemble more those of the porphyrin in solution than those in solid state. This suggests that the porphyrin units are well distributed inside the CN matrix, not forming aggregates, and constitutes a further confirmation of the conservation of the porphyrin structure inside the polymer. Finally, the spectrum of the CN and CuPor physical mixture was acquired and compared to the spectrum of the single components and the CuPor-CN hybrid. As observed, the spectrum is the sum of the spectra of the single components. The small intensity of

the porphyrin bands is related to the small amount of this unit in the mixture (3.8 wt% as in the hybrid) and probably to their agglomeration, as observed for the CuPor spectrum in solid state. This result highlights the importance of the introduction of the porphyrin units in the CN matrix that allows a well distribution and avoids their aggregation.

The catalytic activity of the hybrid material toward the CO_2RR was studied by cyclic voltammetry at low negative potentials (Fig. 2a) and high negative potentials (Figure S8b). The comparison of the CVs in Ar- and CO_2-saturated electrolyte reported in Fig. 2a suggests a catalytic behavior of CuPor-CN for CO_2RR due to the increase of the current density and the slight shift of the reduction wave to less negative potentials under CO_2 atmosphere. However, the most interesting result is obtained by performing the CV under light illumination. Under these conditions, a significant increase of the catalytic activity, in terms of lower onset potential and higher current densities, is observed. The enhancement of the catalytic activity by the light can be attributed to the substrate, since the same behavior was observed when carbon nitride was tested in the same conditions (Figure S8a). It is interesting to note the low activity of the commercial CuPor reported in Figure S8b, which could be attributed to the formation of porphyrin aggregates with a co-facial arrangement observed by UV–Vis, while the dispersion of the porphyrin units into the CN matrix results in a significant increase of the catalytic activity.

RRDE studies were carried out to preliminary and qualitatively determine the CO_2 reduction products [34,35]. With this aim, two different types of measurements were performed. First, CVs were recorded at the disk while the Pt ring was hold at a fix potential. Fig. 2b shows the results obtained in Ar- and CO_2-saturated electrolyte. In Ar atmosphere, the oxidation currents detected on the Pt ring at more negative potentials than −0.7 V can only be attributed to the oxidation of hydrogen produced at the electrode from the hydrogen evolution reaction (HER). In CO_2 atmosphere, however, the higher oxidation currents registered from −0.6 V and the different shape of the ring CV suggest the formation of CO_2RR products. Second, the disk was held at different potentials from −0.65 V to −1.15 V, while the Pt ring potential was scanned from + 0.2 V to + 1.6 V to detect (oxidize) and determine the nature of the products. In absence of CO_2, as expected, only the production of hydrogen from the reduction of water occurred (Fig. 2c), since only the wave related to the H_2 oxidation was recorded at the Pt ring [48]. In presence of CO_2 (Fig. 2d), a change of the CVs was observed, suggesting the formation of different reduction products. The decrease of the oxidation currents between + 0.2 V and + 0.6 V, compare to those recorded in Ar atmosphere, indicates the partial inhibition of the HER at the catalyst. In addition, a second oxidation process with peak potential at + 0.85 V was recorded, which can be attributed to the oxidation of formate [34,35,40]. The assignment of this peak to the formation of formate was confirmed by NMR [40] and DEMS analysis (see below).

The RRDE results obtained for the CN substrate, depicted in Figure S9, confirmed that the catalytic sites for formate production are the Cu sites of the porphyrin units, since the oxidation peak relative to this product was not observed on CN in the same potential window.

The confirmation of the CO_2RR products and the determination of the onset potential with high precision were carried out by DEMS measurements. Results are shown in Fig. 2e-g. CVs were recorder at the CuPor-CN electrode, while following the ionic currents associated with a large variety of possible CO_2RR products in order to elucidate the species generated. The signals recorded were $m/z = 2$ (H_2), $m/z = 16$ (CH_4), $m/$

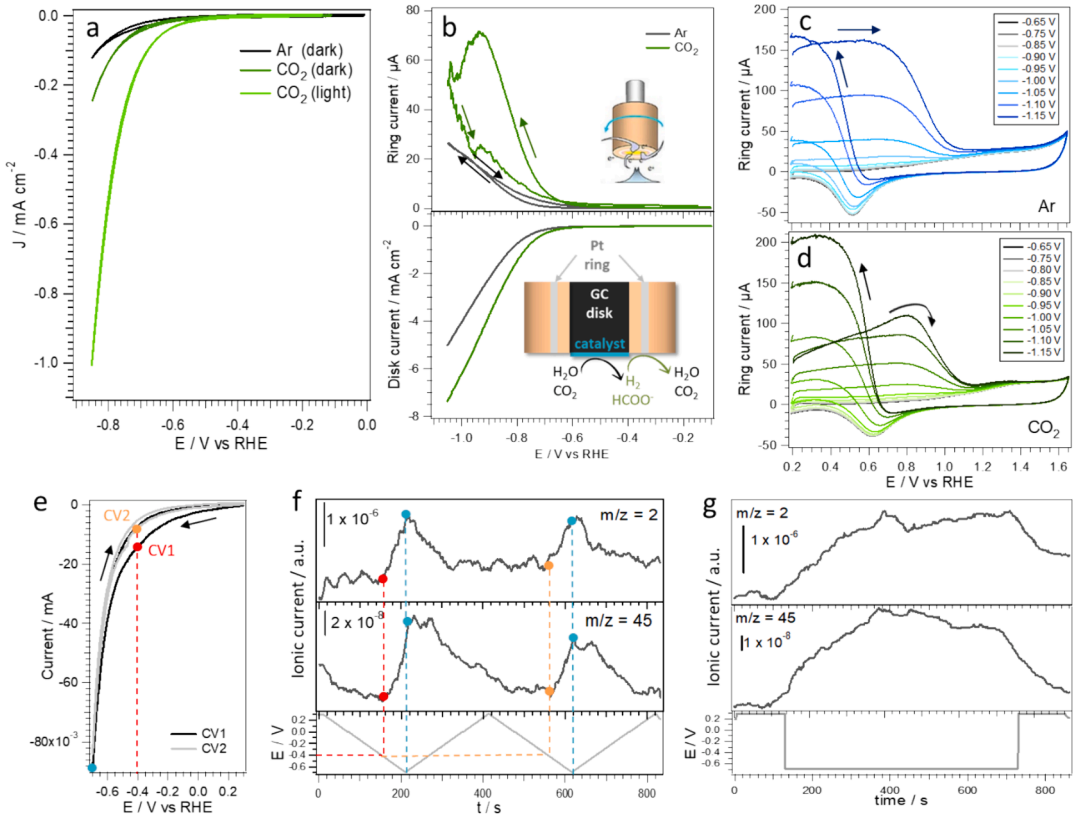

Fig. 2. Electrochemical characterization of CuPor-CN toward the CO_2RR: (a) CVs in Ar- and CO_2-saturated 0.1 M $KHCO_3$ under dark and light illuminating conditions; (b) *I-V* curves recorded at the disk and the ring in dark conditions in Ar- and CO_2-saturated 0.1 M $KHCO_3$ while cycling the disk and holding the ring at + 0.8 V vs RHE; CVs recorded at the ring while holding the disk at different potentials in (c) Ar- and (d) CO_2-saturated 0.1 M $KHCO_3$ under dark conditions; (e) CVs recorded in the DEMS cell and (f) corresponding MSCVs for H_2 ($m/z = 2$) and formate ($m/z = 45$) as a function of the applied potential (bottom panel); and (g) MSTs for H_2 ($m/z = 2$) and formate ($m/z = 45$) at −0.7 V vs RHE. All the measurements shown in (e), (f) and (g) were performed in CO_2-saturated 0.1 M $KHCO_3$ under dark conditions.

$z = 28$ (CO), $m/z = 29$, $m/z = 30$ (C_2H_6), $m/z = 31$ (CH_3O^-) and $m/z = 45$ ($HCOO^-$). In this way, only the m/z signals related to the formation of hydrogen and formate were detected, confirming the RRDE results. The partial inhibition of the HER in presence of CO_2 deduced from the RRDE measurements was also observed by DEMS (Figure S10d). Fig. 2e and 2f show two consecutive CVs recorded at CuPor-CN in CO_2-saturated electrolyte and the corresponding on-line MSCVs for hydrogen ($m/z = 2$) and formate ($m/z = 45$), respectively. The corresponding results obtained in Ar-saturated electrolyte, where only hydrogen was detected, can be found in Figure S10. Two important potentials are highlighted in Fig. 2e, which find their correspondence in Fig. 2f: −0.4 V and −0.7 V. The first one is the potential at which products start to be detected in both cycles and can be identified as the onset potential of the reaction. It is interesting to note that this potential is less negative than the one determined from the conventional CV and RRDE techniques, confirming that DEMS is a high sensitivity technique for both the determination of the products and the onset potential. The second potential is the most negative potential reached during the experiment that corresponds to the peak maximum in the MSCVs.

Fig. 2g reports the m/z signals for hydrogen and formate registered at a fixed potential of −0.7 V (MST). A small delay is observed in the ionic current respect to the applied potential, which can be attributed to the diffusion of the products through the carbon cloth and the membrane. However, a similar profile for both products is obtained. It should be highlighted that, even if CuPor-CN is not 100 % selective towards formate, the fact that hydrogen and formate are obtained in different phases (gas and liquid) makes easy their separation and utilization. In addition, the simultaneous production of hydrogen and formate (hydrogen storage element) has been recently proposed as a novel concept for the continuous (24 h/day) production of hydrogen [49].

Analogous DEMS measurements were performed on the CN substrate (Figure S11) and the commercial CuPor (Figure S12), and interesting outcomes arose from these results. Results for CN agreed with the RRDE measurements. Only hydrogen was detected both in absence and in presence of CO_2, confirming that the Cu atoms are the catalytic sites for the CO_2 reduction. A partial inhibition of the hydrogen produced in presence of CO_2 (49 % less) suggests that CN is able to adsorb CO_2, but it is not able to reduce it in the potential range studied. In the case of CuPor, hydrogen and formate were the only species detected, as on CuPor-CN. However, the $H_2/HCOO^-$ ratio was 2.6-fold higher than that obtained with the hybrid catalyst. This suggests that HER is more favored than CO_2RR on CuPor than on CuPor-CN. This result can be attributed to a synergetic effect between the CN substrate and the copper porphyrin in the hybrid material. This could be explained by the fact that CN adsorbs CO_2, increasing in this way the local concentration of CO_2 near the catalytic Cu sites, which favors the CO_2RR and inhibits the HER.

Finally, the stability under CO_2RR conditions of the CuPor units embedded in the CN matrix was investigated by operando XAS. The results are reported in Fig. 3. Figs. 3a and b show the XANES and the corresponding FT-EXAFS spectra of the CuPor-CN sample in different environments and conditions. No significant changes were observed

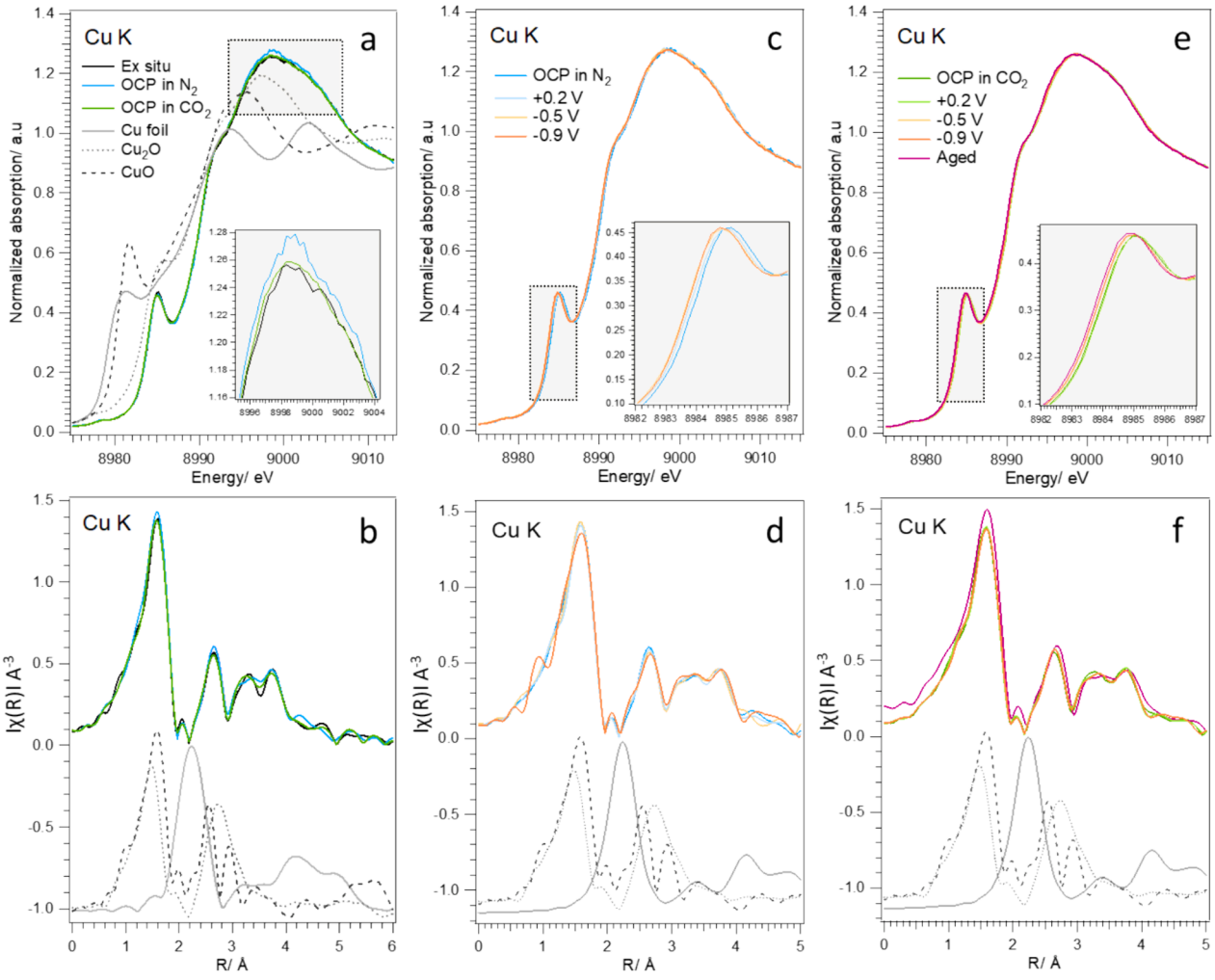

Fig. 3. *In situ* XAS measurements on CuPor-CN: (a,c,e) XANES and (b,d,f) corresponding FT EXAFS spectra at the Cu K edge for CuPor-CN in N_2– (c,d) and CO_2-saturated 0.1 M $KHCO_3$ (e,f) at different applied potentials.

when the sample was introduced in the electrolyte, both in presence and absence of CO_2, with respect to the *ex situ* spectra, indicating that the CuPor unit is stable in the electrolyte. A slight increase of the white line was observed for the sample in N_2-saturated electrolyte, which could be attributed to the adsorption of –OH groups from the electrolyte under open-circuit conditions. This local environment change of the Cu atoms was also observed in the FT-EXAFS spectra (Fig. 3b). The intensity of the peak at 1.6 Å, assigned to Cu–N and/or Cu–O coordination, slightly increased for the sample in nitrogen atmosphere, in agreement with the adsorption of –OH groups. This phenomenon was not observed in presence of CO_2, probably due to the adsorption of CO_2 on the Cu atoms, preventing the adsorption of –OH groups.

The effect of the applied potential was first studied in the absence of CO_2 and results are shown in Figs. 3c and d. The XANES spectra did not suffer any significant change down to −0.9 V. Only a slight shift of the pre-peak energy was observed as the potential became more negative (inset of Fig. 3c), suggesting a slight reduction of the Cu atoms. However, the reduction of Cu(II) to Cu(I) or Cu(0) was not observed from our XAS data. This result is in agreement with the absence of redox peaks associated to the CuPor units in the CVs (Figure S13). In the literature, on the contrary, the reduction of Cu(II) to metallic Cu and the consequent formation of nanoparticles has been reported for similar materials at potentials more negative than −0.6 V [25,29–32]. It has to be highlighted that it was not possible to acquire the XAS measurements at more negative potentials than −0.9 V due to the massive formation of bubbles. Therefore, we cannot completely exclude the demetallation of the porphyrin units and the formation of small nanoparticles at more negative potentials. However, we did not observe the formation of CH_4 or C_2H_4 products, typically obtained with Cu particles [50], which also supports the fact that the CuPor structure in the CN matrix was preserved under CO_2RR conditions.

Similar results were obtained in presence of CO_2, as reported in Figs. 3e and f. No changes were evident in the XANES or FT EXAFS spectra when the potential decreased from the OCP to −0.9 V, apart from a slight shift of the pre-edge peak toward lower energies suggesting a slight reduction of Cu. Also in this case, the reduction of Cu(II) to Cu(I) or Cu(0) and the formation of small nanoparticles was not observed under these conditions. Long-term stability of the CuPor-CN sample is also reported in Figs. 3e and f. XAS measurements were performed on an aged electrode, which did not show significant changes, confirming the structural stability of the copper porphyrin units embedded in the CN matrix in the potential range between + 0.2 V and −0.9 V vs RHE. It has to be considered that the AAT treatment was performed under potential control conditions and an anodic potential that could favour the dissolution of the Cu nanoparticles formed was never applied. For this reason, we exclude that the absence of Cu nanoparticles is due to their electrochemical dissolution [51]. Moreover, the electrolyte was analyzed after 2 h of electrolysis at −1.0 V vs RHE by ICP-MS. The ICP-MS measurements did not revealed the presence of Cu species in the electrolyte.

The stability of the CN substrate, on the other hand, was investigated by XPS. Figure S14 reports the C 1 s and N 1 s XPS regions for the CuPor-CN sample before and after the ageing treatment. The presence of a peak at about 288 eV in the C 1 s region confirms the stability of the CN substrate, since this peak is characteristic of carbon nitride materials [39,40]. In the N 1 s region, the same components and similar ratios are observed in the fresh and cycled samples, suggesting the stability of both the CN substrate and the CuPor units. The components at 398.4 eV and 400.4 eV are related to C = N-C and N-$(C)_3$ species from the CN substrate, while the component at 399.3 eV results from the overlapping of the C-N–H species of the CN and the Cu–N interaction in the CuPor units. In addition, a small component at 401.3 eV related to the expected Teller effect for copper porphyrins can be seen.

4. Conclusions

The results here reported evidence the successful preparation of a catalytic hybrid system by a novel one-step synthesis method. Copper-porphyrin has been covalently introduced in the CN structure by copolymerization. An in-depth characterization of the physicochemical and optical properties of the hybrid systems has been performed, confirming the stability of the porphyrin structure inside the carbon nitride matrix. Benefiting from the presence of the Cu single sites and the photoactivity of the CN substrate, the hybrid system was tested as (photo)electrocatalyst for the CO_2 reduction reaction (CO_2RR). Catalytic tests of the hybrid system and the single components confirmed the high activity of the hybrid toward the CO_2RR and the synergy between the two components. A higher amount of formate was obtained on the hybrid system than on the copper porphyrin alone, which can be attributed to the higher local concentration of CO_2 near the catalytic Cu sites thanks to the CO_2 adsorption on CN, which favors the CO_2RR and inhibits the HER. Finally, the stability of the copper porphyrin units inside the CN matrix was confirmed by *in situ* XAS measurements that did not show the reduction of the Cu sites nor the formation of metal nanoparticles under catalytic conditions.

CRediT authorship contribution statement

Claudio Cometto: Writing – original draft, Methodology, Investigation, Formal analysis. **Giulia Marafon:** Writing – original draft, Methodology, Investigation. **Verónica Celorrio:** Writing – review & editing, Methodology, Investigation. **Gonzalo García:** Writing – review & editing, Methodology, Investigation, Conceptualization. **Steffi Y. Woo:** Writing – original draft, Investigation, Formal analysis. **Enrico Paron:** Investigation. **Alberto Zobelli:** Writing – review & editing, Supervision, Investigation. **Gregorio Bottaro:** Writing – review & editing, Investigation. **Lidia Armelao:** Writing – review & editing, Supervision. **Elena Pastor:** Writing – review & editing, Supervision, Funding acquisition. **Alessandro Moretto:** Writing – review & editing, Supervision, Methodology, Investigation. **Laura Calvillo:** Writing – review & editing, Supervision, Investigation, Funding acquisition, Formal analysis, Conceptualization.

Declaration of competing interest

The authors declare that they have no known competing financial interests or personal relationships that could have appeared to influence the work reported in this paper.

Data availability

Data will be made available on request.

Acknowledgements

This work was financially supported by the University of Padova, Italy (P-DiSC#06BIRD2017-UNIPD), the National Recovery and Resilience Plan (NRRP), by the Ministero dell'Università e della Ricerca (MUR) Italy, funded by the European Union – Next Generation EU (RECYCLE-CO2, PRIN2022-2022FM3LXT), and the Project Junta de Andalucía - Consejería de Universidad, Investigación e Innovación, Spain (P21_00208). EP and GG acknowledge MCIN for funding under project PID2020-117586RB-I00 (MCIN/AEI/10.13039/501100011033). Authors would like to thank the Diamond Light Source for provision of beamtime (SP19850).

Appendix A. Supplementary data

Supplementary data to this article can be found online at https://doi.org/10.1016/j.jcat.2024.115597.

References

[1] J. Liu, H. Shi, Q. Shen, C. Guo, G. Zhao, Green Chem. 19 (2017) 5900–5910.
[2] D.H. Wang, J.N. Pan, H.H. Li, J.J. Liu, Y.B. Wang, L.T. Kang, J.N. Yao, J. Mater. Chem. A 4 (2016) 290–296.
[3] S. Mei, J. Gao, Y. Zhang, J. Yang, Y. Wu, X. Wang, R. Zhao, X. Zhai, C. Hao, R. Li, J. Yan, J. Colloid Interface Sci. 506 (2017) 58–65.
[4] S. Tian, S. Chen, X. Ren, R. Cao, H. Hu, F. Bai, Nano Res. 12 (2019) 3109–3115.
[5] D. Chen, K. Wang, W. Hong, R. Zong, W. Yao, Y. Zhu, Appl. Catal. b: Environ. 166–167 (2015) 366–373.
[6] W.-J. Ong, L.-L. Tan, Y.H. Ng, S.-T. Yong, S.-P. Chai, Chem. Rev. 116 (2016) 7159.
[7] T.S. Miller, A.B. Jorge, T.M. Suter, A. Sella, F. Corà, P.F. McMillan, Phys. Chem. Chem. Phys. 19 (2017) 15613–15638.
[8] Z. Sun, H. Wanga, Z. Wua, L. Wang, Catal. Today 300 (2018) 160–172.
[9] F.K. Kessler, Y. Zheng, D. Schwarz, C. Merschjann, W. Schnick, X. Wang, M. J. Bojdys, Nat. Rev. Mater. 2 (2017) e17030.
[10] R.C. Dante, P. Martin-Ramos, A. Correa-Guimaraes, J. Martin-Gil, Mater. Chem. Phys. 130 (2011) 1094–1102.
[11] J.P. Kelly, R. Kanakala, O.A. Graeve, J. Am. Ceram. Soc. 93 (2010) 3035–3038.
[12] Z. Mo, X. She, Y. Li, L. Liu, L. Huang, Z. Chen, Q. Zhang, H. Xu, H. Li, RSC Adv. 5 (2015) 101552–101562.
[13] C. Collins, N. Thadhani, Z. Iqbal, Carbon 39 (2001) 1175–1181.
[14] J. Liu, T. Sekine, T. Kobayashi, Solid State Commun. 137 (2006) 21–25.
[15] K. Schwinghammer, B. Tuffy, M.B. Mesch, E. Wirnhier, C. Martineau, F. Taulelle, W. Schnick, J. Senker, B.V. Lotsch, Angew. Chem. Int. Ed. 52 (2013) 2435–2439.
[16] M.K. Bhunia, K. Yamauchi, K. Takanabe, Angew. Chem. Int. Ed. 53 (2014) 11001–11005.
[17] M. Zhu, Ji. Chen, L. Huang, R. Ye, J. Xu, Y.-F. Han, Angew. Chem. Int. Ed. 58 (2019) 6595–6599.
[18] J. Wang, X. Huang, Sh. Xi, M. Jo, C. Lee, Y. Wang, X.W. Du, Angew. Chem. Int. Ed. 58 (2019) 13532–13539.
[19] S. Roy, E. Reisner, Angew. Chem. Int. Ed. 58 (2019) 12180–12184.
[20] G. Zhao, H. Pang, G. Liu, P. Li, H. Liu, H. Zhang, L. Shi, J. Ye, Appl. Catal. b: Environ. 200 (2017) 141–149.
[21] B. Ma, M. Blanco, L. Calvillo, L. Chen, G. Chen, T.-C. Lau, G. Dražić, J. Bonin, M. Robert, G. Granozzi, J. Am. Chem. Soc. 143 (2021) 8414–8425.
[22] A. Call, M. Cibian, K. Yamamoto, T. Nakazono, K. Yamauchi, K. Sakai, ACS Catal. 9 (2019) 4867–4874.
[23] M. Fang, L. Xu, H. Zhang, Y. Zhu, W.-Y. Wong, J. Am. Chem. Soc. 144 (2022) 15143–15154.
[24] M. Wang, K. Torbensen, D. Salvatore, S. Ren, D. Joulié, F. Dumoulin, D. Mendoza, B. Lassalle-Kaiser, U. Işci, C.P. Berlinguette, M. Robert, Nature Commun. 10 (2019) e3602.
[25] D. Karapinar, A. Zitolo, T.N. Huan, S. Zanna, D. Taverna, L.H.G. Tizei, D. Giaume, P. Marcus, V. Mougel, M. Fontecave, ChemSusChem 13 (2020) 173–179.
[26] P. Gotico, Z. Halime, A. Aukauloo, Dalton Trans. 49 (2020) 2381–2396.
[27] P. Yu, X. Lv, Q. Wang, H. Huang, W. Weng, C. Peng, L. Zhang, G. Zheng, Small 19 (2023) e2205730.
[28] Y.Y. Birdja, J. Shen, M.T.M. Koper, Catal. Today 288 (2017) 37–47.
[29] X. Su, Z. Jiang, J. Zhou, H. Liu, D. Zhou, H. Shang, X. Ni, Z. Peng, F. Yang, W. Chen, Z. Qi, D. Wang, Y. Wang, Nature Commun. 13 (2022) e1322.
[30] Z. Weng, Y. Wu, M. Wang, J. Jiang, K. Yang, S. Huo, X.-F. Wang, Q. Ma, G. W. Brudvig, V.S. Batista, Y. Liang, Z. Feng, H. Wang, Nature Commun. 9 (2018) e415.
[31] D. Karapinar, N.T. Huan, N.R. Sahraie, J. Li, D. Wakerley, N. Touati, S. Zanna, D. Taverna, L.H. Galvão Tizei, A. Zitolo, F. Jaouen, V. Mougel, M. Fontecave, Angew Chem. Int. Ed. 58 (2019) 14775–15158.
[32] L. Ma, W. Hu, B. Mei, H. Liu, B. Yuan, J. Zang, T. Chen, L. Zou, Z. Zou, B. Yang, Y. Yu, J. Ma, Z. Jiang, K. Wen, H. Yang, ACS Catal. 10 (2020) 4534–4542.
[33] J. Zhang, X. Chen, K. Takanabe, K. Maeda, K. Domen, J.D. Epping, X. Fu, M. Antonietti, X. Wang, Angew. Chem. Int. Ed. 49 (2010) 441–444.
[34] F. Zhang, A.C. Co, J. Electrochem. Soc. 167 (2020) e046517.
[35] X. Zhu, K. Gupta, M. Bersani, J.A. Darr, P.R. Shearing, D.J.L. Brett, Electrochim. Acta 283 (2018) 1037–1044.
[36] S. Pérez-Rodríguez, M. Corengia, G. García, C.F. Zinola, M.J. Lázaro, E. Pastor, Inter. J. Hydrogen Energ. 37 (2012) 7141–7151.
[37] H. Nagatani, H. Tanida, I. Watanabe, T. Sagara, Anal. Sci. 25 (2009) 475–480.
[38] M. Saphier, T. Yifrah, I. Zilbermanna, O. Saphier, A.I. Shames, N. Froumin, D. Meyerstein, D.M. Guldi, J. Porphyrins Phthalocyanines 16 (2012) 1124–1131.
[39] Q. Liang, Z. Li, Z.-H. Huang, F. Kang, Q.-H. Yang, Adv. Funct. Mater. 25 (2015) 6885–6892.
[40] C. Cometto, A. Ugolotti, E. Grazietti, A. Moretto, G. Bottaro, L. Armelao, C. Di Valentin, L. Calvillo, G. Granozzi, npj 2D Mater. Appl. 5 (2021) e63.
[41] K. Diller, F. Klappenberger, M. Marschall, K. Hermann, A. Nefedov, Ch. Wöll, J. V. Barth, J. Chem. Phys. 136 (2012) e014705.
[42] G. Zhang, A. Savateev, Y. Zhao, L. Li, M. Antonietti, J. Mater. Chem. A 5 (2017) 12723–12728.
[43] A.A. Sinelshchikova, S.E. Nefedov, Y.Y. Enakieva, Y.G. Gorbunova, A.Y. Tsivadze, K.M. Kadish, P. Chen, A. Bessmertnykh-Lemeune, C. Stern, R. Guilard, Inorg. Chem. 52 (2013) 999–1008.
[44] R. van Hameren, A.M. van Buul, M.A. Castriciano, V. Villari, N. Micali, P. Schön, S. Speller, L. Monsù Scolaro, A.E. Rowan, J.A.A.W. Elemans, R.J.M. Nolte, Nano Lett. 8 (2008) 253–259.
[45] D. Chena, K. Wanga, W. Honga, R. Zong, W. Yao, Y. Zhu, Appl. Catal. B: Environ. 166–167 (2015) 366–373.
[46] M. Vasilopoulou, D.G. Georgiadou, A.M. Douvas, A. Soultati, V. Constantoudis, D. Davazoglou, S. Gardelis, L.C. Palilis, M. Fakis, S. Kennou, T. Lazarides, A. G. Coutsolelos, P. Argitis, J. Mater. Chem. A 2 (2014) 182–192.
[47] D. Vidyasagar, S.G. Ghugal, S.S. Umare, M. Banavoth, Sci. Reports 9 (2019) 7186.
[48] V. Briega-Martos, A. Ferre-Vilaplana, E. Herrero, J.M. Feliu, Electrochim. Acta 354 (2020) e136620.
[49] C. Ampelli, D. Giusi, M. Miceli, T. Merdzhanova, V. Smirnov, U. Chime, O. Astakhov, A.J. Martín, F.L.P. Veenstra, F.A. Garcés Pineda, J. González-Cobos, M. García-Tecedor, S. Giménez, W. Jaegermann, G. Centi, J. Pérez-Ramírez, J. R. Galán-Mascarós, S. Perathoner, Energy Environ. Sci. 16 (2023) 1644–1661.
[50] S. Nitopi, E. Bertheussen, S.B. Scott, X. Liu, A.K. Engstfeld, S. Horch, B. Seger, I.E. L. Stephens, K. Chan, C. Hahn, J.K. Nørskov, T.F. Jaramillo, I. Chorkendorff, Chem. Rev. 119 (2019) 7610–7672.
[51] E. Boutin, A. Salamé, M. Robert, Nat. Commun. 13 (2022) e4190.